Bioactive Materials 48 (2025) 43–54

Contents lists available at ScienceDirect

Bioactive Materials

journal homepage: www.keaipublishing.com/en/journals/bioactive-materials

MiR-19-loaded oxidative stress-relief microgels with immunomodulatory and regeneration functions to reduce cardiac remodeling after myocardial infarction

Kai Wang [a,c,1], Jun Wen [b,1], Wen-Yao Wang [b,1], Kefei Zhao [c,e,1], Tong Zhou [c], Shunqin Wang [c], Qiaoxuan Wang [c], Liyin Shen [c], Yanxin Xiang [e], Tanchen Ren [a], Jinghai Chen [d,**], Yi-Da Tang [b,***], Yang Zhu [a,c,****], Changyou Gao [a,c,e,*]

[a] The State Key Laboratory of Transvascular Implantation Devices, The Second Affiliated Hospital, Zhejiang University, Hangzhou, 310009, China
[b] Department of Cardiology and Institute of Vascular Medicine, Peking University Third Hospital, Key Laboratory of Molecular Cardiovascular Science, Ministry of Education, Beijing, 100191, China
[c] MOE Key Laboratory of Macromolecular Synthesis and Functionalization, Department of Polymer Science and Engineering, Zhejiang University, Hangzhou, 310058, China
[d] Department of Cardiology, The Second Affiliated Hospital, Institute of Translational Medicine, Zhejiang University School of Medicine, Hangzhou, 310009, China
[e] Center for Healthcare Materials, Shaoxing Institute, Zhejiang University, Shaoxing, 312099, China

ARTICLE INFO

Keywords:
Microgels
Cardiomyocyte regeneration
Myocardial infarction
microRNA
Inflammation

ABSTRACT

Regeneration therapeutic strategy by microRNAs for boosting cardiomyocyte proliferation in treating myocardial infarction (MI) has the challenges of efficient delivery, and toxicity and risk of sudden death. Herein, oxidative stress-relief microgels were developed for miR-19a/b delivery, modulation of inflammatory tissue microenvironment, promotion of cardiomyocyte proliferation, and maintenance of heart function post MI. The cholesterol-modified miR-19a/b was encapsulated into the cavity of β-cyclodextrin in selenoketal-containing microgels. The microgels could effectively scavenge typical reactive oxygen species (ROS), and down-regulate the intracellular ROS level and the levels of typical inflammatory factors. The microgels could improve the acute inflammatory microenvironment for better cardiomyocyte survival and cellular uptake of miR-19a/b, leading to significant promotion of cardiomyocyte proliferation *in vivo*. In the rat and minipig models of MI, the microgels most effectively inhibited the acute inflammatory response and reduced the cardiomyocytes apoptosis, resulting in a significant improvement of cardiac function and restriction of pathological remodeling post MI, and thereby best heart function revealed by echocardiography and histological analysis.

1. Introduction

Myocardial infarction (MI) is one of the major causes of disability even death worldwide [1–3]. The irreversible damage to cardiomyocytes caused by myocardial infarction would deteriorate heart function, leading to heart failure and eventual death [4,5]. Unlike newborn mammalian hearts, adult mammalian hearts have almost lost their capability to regenerate, thus scar tissue would be formed post MI. The formation of scars would block the blood supply to the heart, leading to more cardiomyocyte death, loss of muscle tissue, and heart failure [6,7]. Current treatments mainly focus on removing the blockage and restoring blood supply to the damaged myocardium [8]. However,

Peer review under the responsibility of KeAi Communications Co., Ltd.
* Corresponding authors. The State Key Laboratory of Transvascular Implantation Devices, The Second Affiliated Hospital, Zhejiang University, Hangzhou, 310009, China.
** Corresponding author.
*** Corresponding author.
**** Corresponding author. The State Key Laboratory of Transvascular Implantation Devices, The Second Affiliated Hospital, Zhejiang University, Hangzhou, 310009, China.
E-mail addresses: jinghaichen@zju.edu.cn (J. Chen), tangyida@bjmu.edu.cn (Y.-D. Tang), zhuyang@zju.edu.cn (Y. Zhu), cygao@zju.edu.cn (C. Gao).
[1] These authors contributed equally to this work.

https://doi.org/10.1016/j.bioactmat.2025.02.004
Received 12 October 2024; Received in revised form 14 January 2025; Accepted 2 February 2025
Available online 13 February 2025

they are insufficient to fully restore blood flow and realize complete cardiac repair [9].

MicroRNAs (miRNAs), a class of short, non-coding single-stranded RNA molecules are encoded by ~22-nucleotide long endogenous genes, which play a key role in numerous biological events, including cardiomyocyte proliferation and heart development [10–12]. The cardiac cells-specific miRNAs can induce cardiac regeneration and cardiomyocyte proliferation [13]. For example, the miR302-367 cluster was found to promote cardiomyocyte proliferation and heart regeneration by directly regulating the Hippo/Yap pathway. The local delivery of adeno-associated virus serotype 6 (AAV6)-miR-199a was also proved to remarkably stimulate the cardiomyocyte proliferation [14]. Recently, we found that miR-19a/b is demonstrated to inhibit the expression of phosphatase and tensin homolog (PTEN), and thereby to enhance the cardiomyocyte proliferation and promote the cardiac regeneration [15,16].

Because of the poor stability and permeability of exposed miRNAs *in vivo*, it is necessary to find effective miRNAs delivery systems, including the viral vectors and nonviral vectors [17] with different pros and cons. Although the non-viral lipid-based nanocarriers are safer for miRNAs delivery *in vivo*, their organotoxicity and targeting selectivity are still challenging [9,18]. Hydrogel-based nonviral gene delivery systems have become an available strategy in various scenarios of regenerative medicine [19,20]. For example, an injectable hyaluronic acid (HA) hydrogel loaded with miR-302 mimics promotes cardiomyocyte proliferation in rat post-MI [21].

Numerous explorations of functional hydrogels have been performed on MI treatment, among which the reactive oxygen species (ROS)-eliminating hydrogels can are one of the effective candidates to modulate inflammatory MI microenvironment by reducing the harmful ROS contents in the very earlier stage, and thereby better maintain the cardiomyocyte survival and MI therapy [22–26]. Nonetheless, the traditional bulk hydrogels are often characterized by a relatively large size with a low surface/volume ratio and nanoporous structure, leading to the relatively poor injectability and sensitivity to the stimuli of tissue microenvironment [27,28], and insufficient nutrient and oxygen exchange. Consequently, they are disadvantageous for cell infiltration, vascularization and long-term cell proliferation.

In this study, we propose oxidative stress-relief microgels as a delivery system of miR-19a/b for enhanced cardiomyocyte proliferation and cardiac repair in rats and pigs (Scheme 1). The microgels can be precisely delivered to the injured tissues via a minimally invasive pathway [28–30]. Their relatively large surface/volume ratio and large pores in-between the microgels are favorable to enhance the transportation of nutrients and oxygen, guide cell ingrowth and tissue formation, alongside with their degradation. To reverse the harsh oxidative microenvironment post MI and thereby protect cardiomyocyte against apoptosis, selenoketal that is extremely sensitive to reactive oxygen species (ROS) is used to construct the ROS-scavenging microgels. The oxidative stress-relief microgels with miR-19a/b is expected to achieve better cardiomyocyte proliferation, eventually contributing to a significant cardiac function improvement and myocardial fibrosis inhibition than the bulk counterpart (Scheme 1). The significantly increased regeneration signals and outstanding therapeutic effect are further demonstrated in minipigs post MI *in vivo*, revealing a significant progress for treatment of MI in human being.

2. Results

2.1. Preparation of ROS-scavenging M gel loaded with miR-19a/b

The preparation of extremely ROS-sensitive microgels relied on the

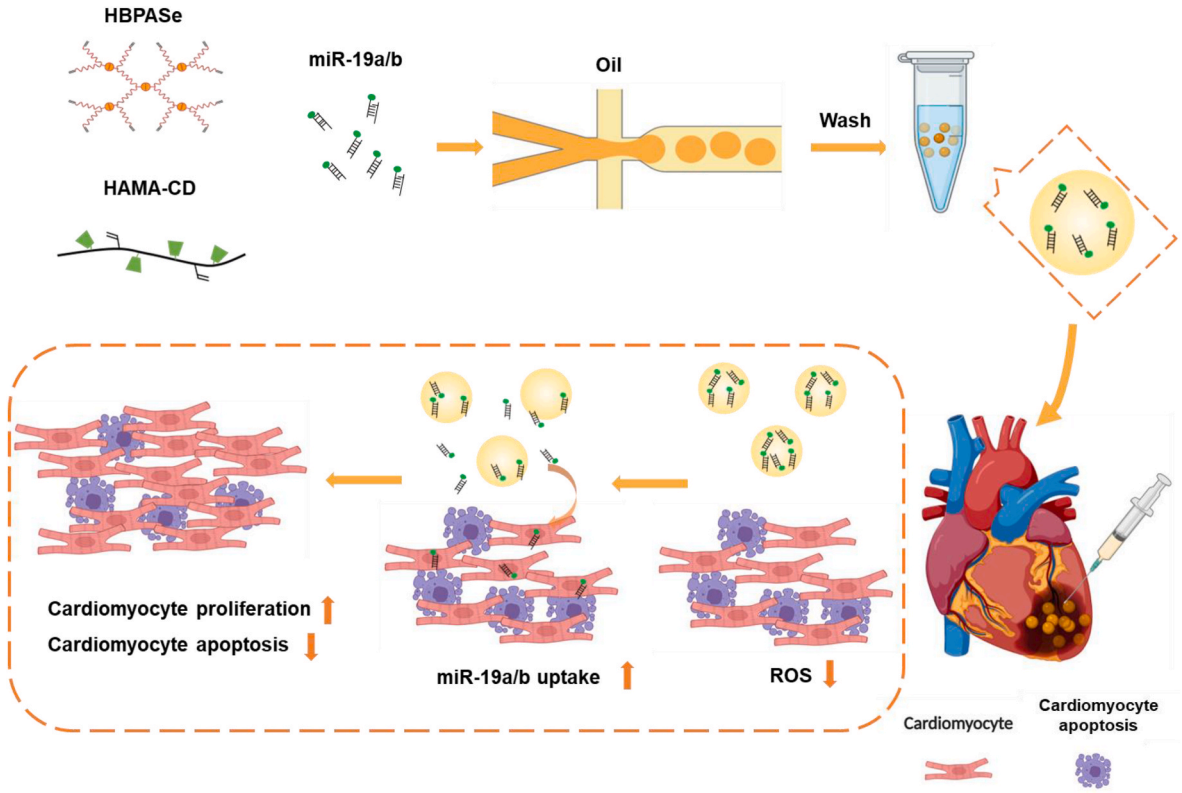

Scheme 1. Schematic illustration of ROS-responsive microgels loaded with miR-19a/b (M gel) for promoting cardiomyocyte proliferation *in vivo*. Preparation of M gel building blocks by encapsulating miR-19a/b into ROS-scavenging microgels in a microfluidic device. The microgels are formed by crosslinking the precursor solutions of HBPASe and HAMA-CD macromolecules. The miR-19a/b modified with cholesterol is loaded into the cavity of cyclodextrin of HAMA-CD. This system can sensitively scavenge the locally overproduced ROS in the MI microenvironment, continuously release the miR-19a/b, and improve cellular uptake of miR-19a/b for efficiently stimulating the proliferation of cardiomyocytes and reducing apoptosis.

use of selenoketal-diamine (selenoketal-NH_2) molecules, which were pioneering synthesized and characterized (Fig. S1, Supporting Information). The -NH_2 groups in selenoketal-NH_2 were then clicked with the carbon double bonds in poly(ethylene glycol) diacrylate (PEGDA) to obtain the double bond end-capped hyperbranched polymers (HBPASe) via a one-step Michael addition reaction (Fig. S2, Supporting Information). To incorporate the miR-19a/b via a host-guest interaction, cholesterol-modified miR-19a/b was loaded into β-cyclodextrin (β-CD) that was grafted on the backbone of methacrylated hyaluronic acid (HAMA-CD, Fig. S3). The 5' end of the passenger strand of miR-19a/b was conjugated with cholesterol, a guest of CD with a binding constant (*Ka*) of 1.7×10^4 M^{-1} [31]. Meanwhile, the cholesterol could further enhance cellular uptake of siRNAs and miRNAs via passive internalization [32,33]. The ROS-responsive microgels were finally constructed with the precursor consisting of HBPASe and HAMA-CD through a microfluidics technology.

Water-in-oil (W/O) single-emulsion droplets were produced to fabricate the ROS-responsive microgels loaded with miR-19a/b (M gel) by using a microfluidic device composed of an inner capillary tube (inner diameter = 0.1 mm) and outer polyvinyl fluoride (ETFE) tube (inner diameter = 0.5 mm). The inner phase was a mixture of HBPASe, HAMA-CD and miR-19a/b solutions, and the outer phase was a mixture of paraffin oil and Span 80. As an important preparation parameter, the flow rates of both outer and inner phases were adjusted to obtain the desired diameters of microgels (Fig. 1a). The sizes of droplets usually increased when the inner flow rate increased or the outer flow rate decreased. The M gels were finally stabilized by crosslinking under UV irradiation in the microfluidic channel. They were uniformly distributed with a spherical morphology and size of ~200 μm (Fig. 1c–e, Movie S1). After freeze-drying, they could still maintain their spherical morphology, accompanying with the apparent interconnected porous structure (Fig. 1d) and shrunk particle size [34]. As a comparison, the bulk hydrogel (B gel) was prepared by UV polymerization of HBPASe, HAMA-CD and miR-19a/b solutions of the same concentrations.

Injection of biomaterials is a favorable route for minimal invasive therapy in clinics [28,35–37]. Although some types of tissues can be directly accessed by a syringe needle, many diseases such as myocardial infarction, neurovascular blockages and tumor treatment often require minimally invasive delivery through long thin catheters in clinical treatments [37–40]. Since catheters are often substantially longer and narrower than syringes, the traditional bulk hydrogels are difficult to meet the demands of minimally invasive delivery. Compared to the B gel that could not be injected through a catheter with a diameter of 0.5 mm, the M gel exhibited great feasibility on injection through the same catheter (Fig. 1b), because the M gel had a relatively smaller storage modulus and exhibited a shear-thinning ability (Fig. S4).

The ROS-scavenging activity and miR-19a/b release were compared between the M gel and B gel. Because the selenoketal bonds are much sensitive under mild oxidative stimuli [41,42], both the M gel and B gel showed a very quick ROS-scavenging ability with respect to reducing 1,

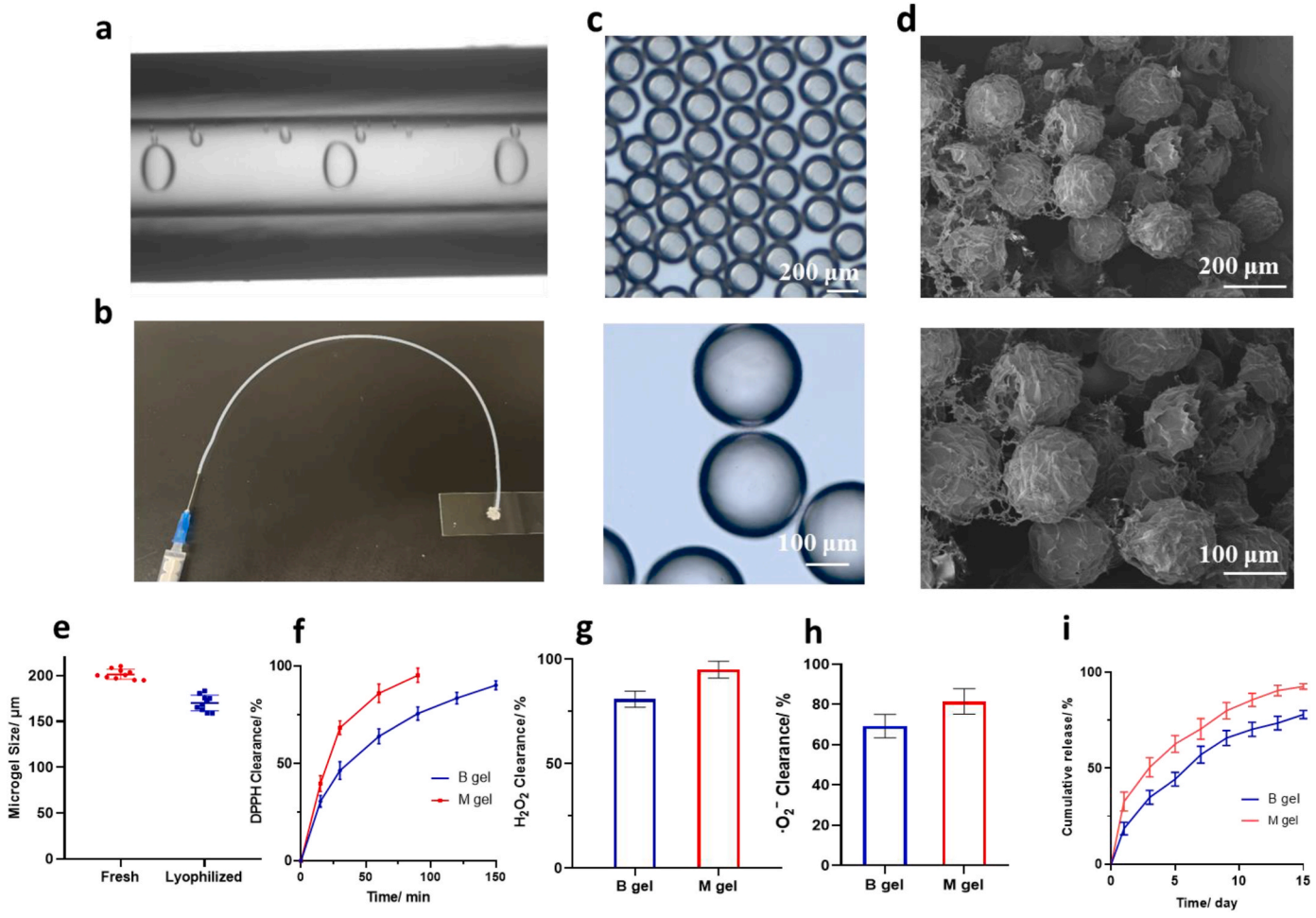

Fig. 1. Physiochemical properties of ROS-responsive microgels loaded with miR-19a/b. (a) Homogeneous droplets formed at a flow focusing junction of the microfluidic channel. (b) Injection of the M gel through a catheter. (c) Optical microscopy images of freshly prepared microgels. (d) SEM images of freeze-dried microgels. (e) Size of freshly prepared and lyophilized microgels. (f) Clearance of DPPH radicals, (g) H_2O_2 and (h) $\cdot O_2^-$ by the bulk hydrogel (B gel) and M gel. (i) Release of cholesterol-modified miR-19a/b from the B gel and M gel in 100 mM H_2O_2 containing DMEM. $n = 3$ per group.

1-diphenyl-2-picrylhydrazyl (DPPH) radicals, H_2O_2 and superoxide anions ($\cdot O_2^-$) (Fig. 1f–h). However, the M gel could scavenge ROS more quickly with a larger specific surface area, where 100 μL of M gel removed over 95 % of 200 μM DPPH radicals within 90 min and 200 μM H_2O_2 within 30 min. Meanwhile, the M gel also exhibited a faster scavenging ability on $\cdot O_2^-$ due to its larger specific surface area and thus the ease of diffusion. The release of miR-19a had the similar tendency, where the M gel resulted in a faster release of miR-19a in H_2O_2 solution, leading to ~62 % and 80 % of miR-19a release at day 5 and day 9, respectively (Fig. 1h). Although the release of miR-19a/b is theoretically governed by the dynamic host-guest interaction between cholesterol and cyclodextrin, the larger specific area of M gel allows a relatively faster release due to the less physical hindrance in diffusion. Due to the great sensitivity of B gel and M gel on ROS, they both exhibited a relatively fast degradation behavior in H_2O_2/PBS solution compared in pure PBS (Fig. S5).

2.2. ROS-responsive M gel reduced intracellular ROS and maintained cellular uptake of miR-19a/b in vitro

Both the M gel and B gel had no cytotoxicity (Fig. S6). The intracellular ROS-scavenging ability was identified by a ROS indicator 2′,7′-dichlorodihydrofluorescein diacetate (DCFH-DA) [43,44] using the M gel and B gel-treated H9C2 cells in a H_2O_2 environment *in vitro* (Fig. 2a). Flow cytometry demonstrated that ROS was increased in cells under H_2O_2 stimulus. By contrast, the intracellular ROS was down-regulated significantly under the existence of B gel and especially M gel due to the effective ROS-scavenging ability (Fig. 2b, Fig. S7). The ROS level in the M gel group was down-regulated to a similar level of the control group without H_2O_2. Furthermore, Fig. 2c shows that the cellular uptake of Cy3-modified miR-19a (miR-19a-Cy3) in the M gel group was comparable to the control group (miR-19a-Cy3 and H2C9 cells in pure DMEM). It is worth mentioning that the chemical structure of released miRNA should not be changed, thus the use of miR-19a-Cy3 can avoid complexity. Moreover, three-washings ensured the complete removal of free miR-19a-Cy3, so that the fluorescence can be only recorded from the cells with internalized miR-19a-Cy3. By contrast, was hampered in the B gel and H_2O_2 groups. These results reveal that the miR-19 uptake can be well guaranteed in an oxidative stress environment when the M gel exists, likely due to its robust ROS scavenging and cell-protection abilities.

2.3. ROS-responsive M gel reduced inflammation and cell apoptosis in vivo

Next, the M gel and B gel were injected into adult rat infarcted hearts to evaluate their anti-inflammation and anti-apoptosis effects *in vivo* (Fig. 3a). Immunofluorescent staining of CD86 and CD163, markers for pro-inflammatory M1 and anti-inflammatory M2 macrophages, respectively, was performed to detect the phenotypes of macrophages and their distribution in the harvested hearts at day 5. Both the M gel and B gel reduced the portion of M1 macrophages and increased the portion of M2 macrophages compared to the MI group (Fig. 3b–d) [45]. However, the M gel had a significantly higher ratio of M2/M1 macrophages than the B gel, suggesting a better anti-inflammation effect. This observation was further substantiated by the significantly lower expressions of CD86, tumor necrosis factor-α (TNF-α), interleukin-1β (IL-1β) and matrix metalloproteinase-2 (MMP-2). Moreover, the highest expression of anti-inflammation-related gene of CD163 was observed in the M gel group (Fig. 3e). Taken together, the treatment of M gel can significantly reduce the acute MI-induced inflammation.

The best cellular protection effect of M gel *in vivo* was also confirmed by evaluating the cardiomyocyte apoptosis via the TdT-mediated dUTP-biotin nick end labeling (TUNEL) immunostaining assay. Compared to

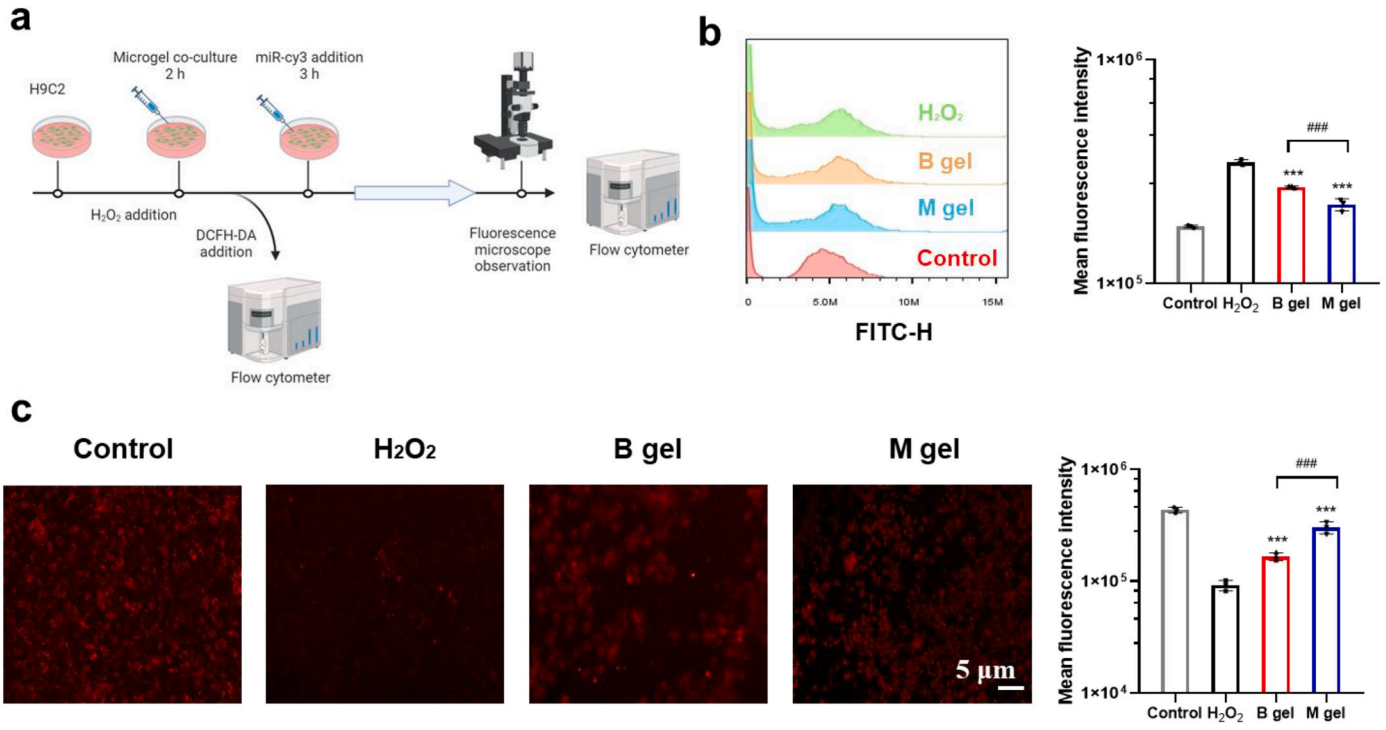

Fig. 2. M gel protects cells against oxidative stress and maintains cellular uptake ability of miR-19a/b. (a) Timeline of the cell model study. (b) Flow cytometry results of H2C9 cells being incubated in 500 μM H_2O_2 and DMEM, and 500 μM H_2O_2 and DMEM with M gel and B gel for 2 h, respectively. (c) Fluorescence intensity of H2C9 cells with internalized miR-19a-Cy3 and quantitative analysis of mean fluorescence intensity (right). Control group: miR-19a-Cy3 and H2C9 cells in pure DMEM; H_2O_2 group: miR-19a-Cy3 and H2C9 cells in DMEM containing 500 μM H_2O_2; M gel group: miR-19a-Cy3 and H2C9 cells in DMEM containing 500 μM H_2O_2 and M gel; B gel group: miR-19a-Cy3 and H2C9 cells in DMEM containing 500 μM H_2O_2 and B gel. $n = 3$ per group. ***p < 0.001 versus control group; ###p < 0.001 between the selected groups.

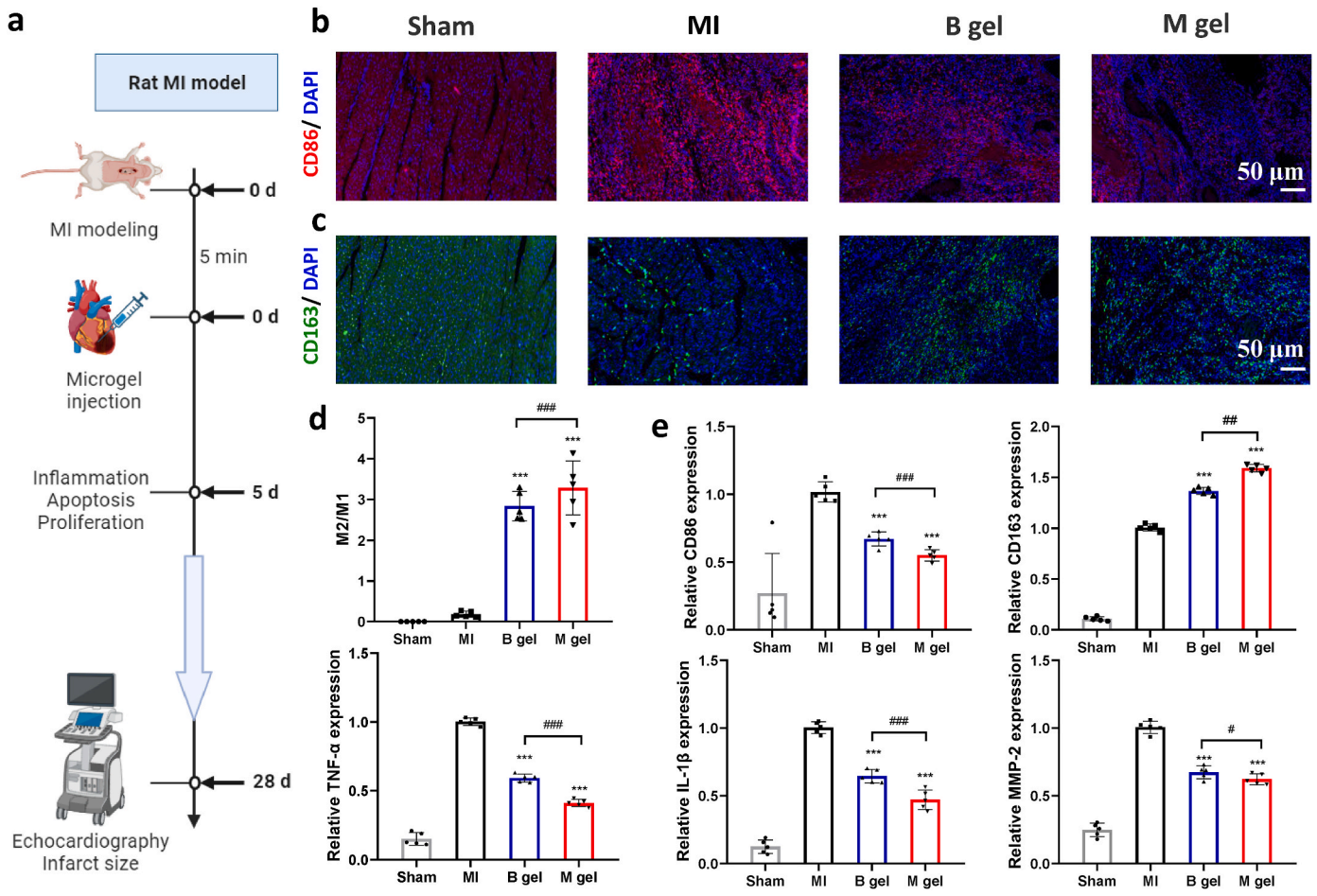

Fig. 3. M gel down-regulates inflammation *in vivo*. (a) Timeline of the rat MI study. Representative (b) CD86 (M1 macrophage marker, red) and (c) CD163 (M2 macrophage marker, green) staining images in infarcted area 5 d post-surgery. Cell nuclei were counter-stained with DAPI (blue). (d) Quantitative analysis of the ratio of M2/M1 macrophages. (e) Expression of inflammation-related genes as marked in the Y-axes. $n = 5$ per group. *p < 0.05 and ***p < 0.001 versus MI group; $^{\#}$p < 0.05, $^{\#\#}$p < 0.01 and $^{\#\#\#}$p < 0.001 between the selected groups.

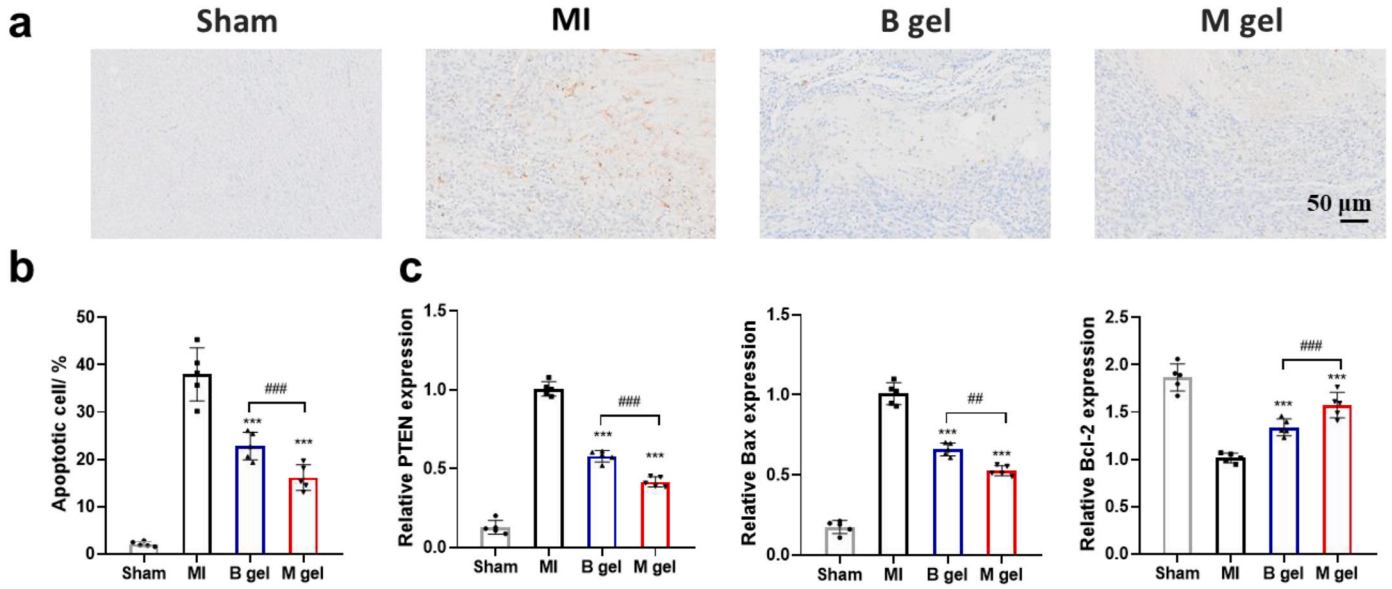

Fig. 4. M gel protects cells against oxidative stress and reduces cell apoptosis *in vivo*. (a) Representative TUNEL staining images of different groups in infarcted area 5 d post-surgery, and (b) quantitative analysis of cell apoptosis. (c) Expression of miR-19a/b targeted gene (PTEN and Bim), and Bcl-2. $n = 5$ per group. ***p < 0.001 versus MI group; $^{\#\#}$p < 0.01 and $^{\#\#\#}$p < 0.001 between the selected groups.

the Sham group, the MI group markedly increased the number of TUNEL-positive cells (Fig. 4a). Notably, the M gel group exhibited significantly fewer apoptotic cells in the infarcted areas than the B gel (Fig. 4b). Moreover, the relative expressions of PTEN and Bim, which are apoptosis-promoted genes [46,47], were both significantly suppressed by the M gel-treated group (Fig. 4c). By contrast, the relative expression of Bcl-2, an anti-apoptosis gene, was most significantly enhanced in the M gel-treated group.

Collectively, the cardiac protection post MI granted by the oxidative stress-relief hydrogel, especially the M gel, can effectively suppress the acute inflammation and reduce cardiomyocyte apoptosis post MI.

2.4. ROS-responsive M gel improved cardiomyocyte proliferation by miR-19a/b post MI

To verify that the early cardiac protection is detrimental to cardiomyocyte proliferation and cardiac regeneration, Ki67 (a biomarker for all stages in the cell cycle) and immunofluorescent staining assays were performed after 5-day post treatments in MI rats, respectively. In the total MI area or healthy myocardium area, there would be no cardiomyocyte under proliferation. Therefore, the border zone between MI area and healthy myocardium area was chosen for analysis, where the cardiomyocytes appeared unusually orderly. The M gel significantly increased the proportion of Ki67^{+}/cardiac troponin T^{+} (cTnT^{+}) cardiomyocytes (~7.67 %) around the injection sites (Fig. 5a), which was much higher than other groups (~3.27 % in the B gel group and ~0.07 % in the MI group) (Fig. 5b). Notably, the degree is infrequently high compared to previous works [48–52] aiming at cardiomyocyte proliferation. Meanwhile, phosphorylated histone H3 (PH3, a biomarker for cells in late G2 and mitosis) and Aurora B kinase (Aurora B, a biomarker of cytokinesis) immunonstaining assay found that the PH3^{+}/cTnT^{+} and Aurora B^{+}/cTnT^{+} cardiomyocytes around the MI site were also significantly higher than all other groups (Fig. 5a and b). This higher percentage of cardiomyocyte regeneration should result from the good retention of M gel, and its robust microenvironment regulation and better cellular uptake of miR-19a/b (Fig. S8). Therefore, the M gel treatment significantly promotes the cardiomyocytes to re-enter the cell cycle and thereby proliferation in the infarcted hearts.

2.5. M gel protected cardiac function and reduced myocardial fibrosis in a rat MI model

Based on the strong ability to suppress inflammation, reduce cardiomyocyte apoptosis and promote cardiomyocyte proliferation by the M gel, a better therapeutic effect post MI is reasonably expected. Echocardiography illustrated that both the M gel and B gel groups reduced the cardiac hypertrophy. The M gel treatment amplified this benefit with the most improved anterior wall movement and decreased

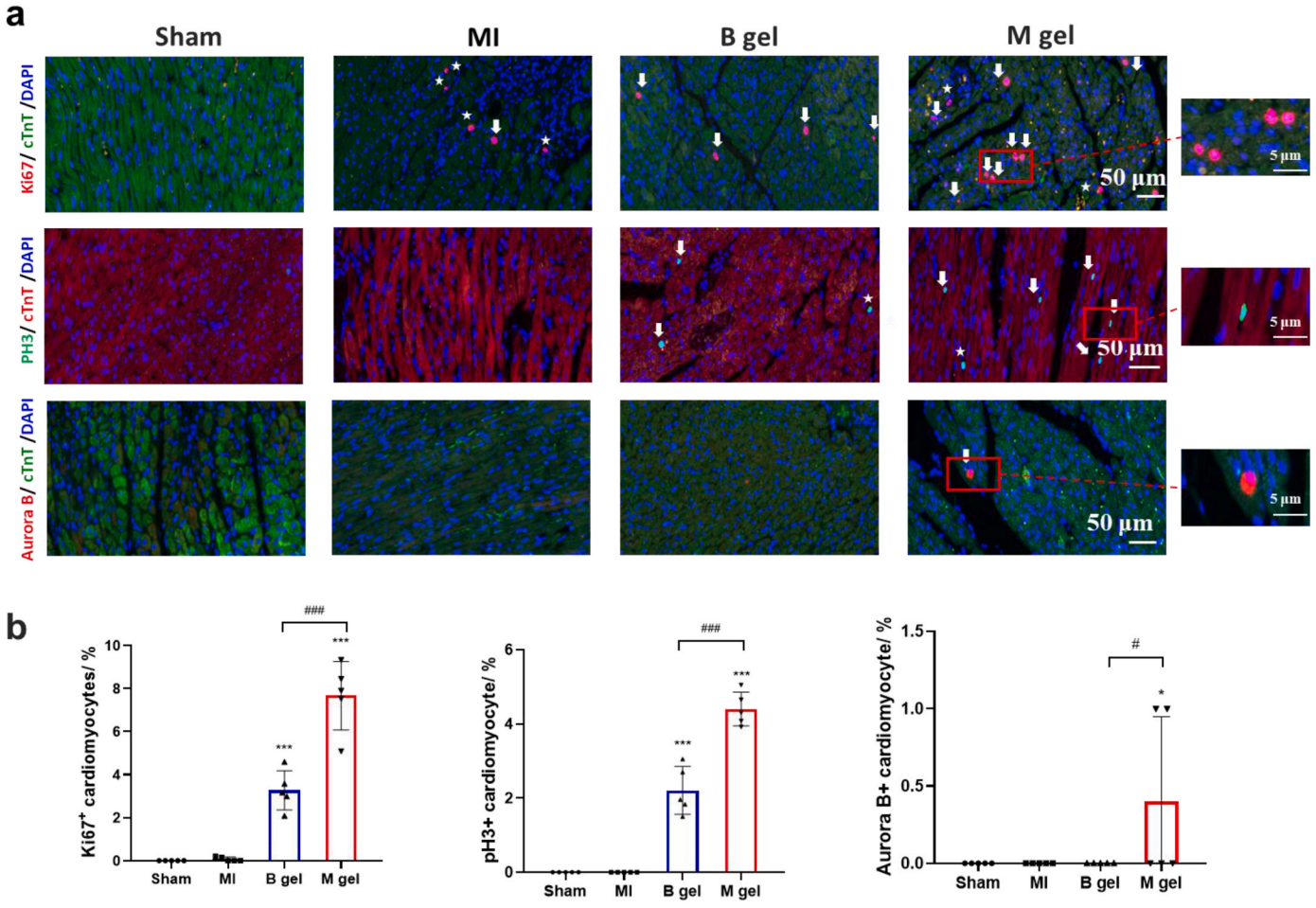

Fig. 5. M gel helps miR-19a/b in promoting cardiomyocyte proliferation *in vivo*. (a) Representative images of Ki67, PH3 and Aurora B staining of cardiomyocytes (white arrows) and non-myocytes (white *) at day 5, demonstrating the increased proliferation in the M gel-treated hearts than the B gel-treated ones. Ki67, cardiac troponin T (cTnT) and DAPI label proliferating cells (red), cardiomyocytes (green), and nuclei (blue), respectively. PH3, cTnT and DAPI label proliferating cells (green), cardiomyocytes (red), and nuclei (blue), respectively. Aurora B, cTnT and DAPI label proliferating cells (green), cardiomyocytes (red), and nuclei (blue), respectively. (b) Relative percentages of Ki67, PH3 and Aurora B-positive cardiomyocytes. $n = 5$ per group. ***$p < 0.001$ versus MI group; $^{\#}p < 0.05$ and $^{\#\#\#}p < 0.001$ between the selected groups.

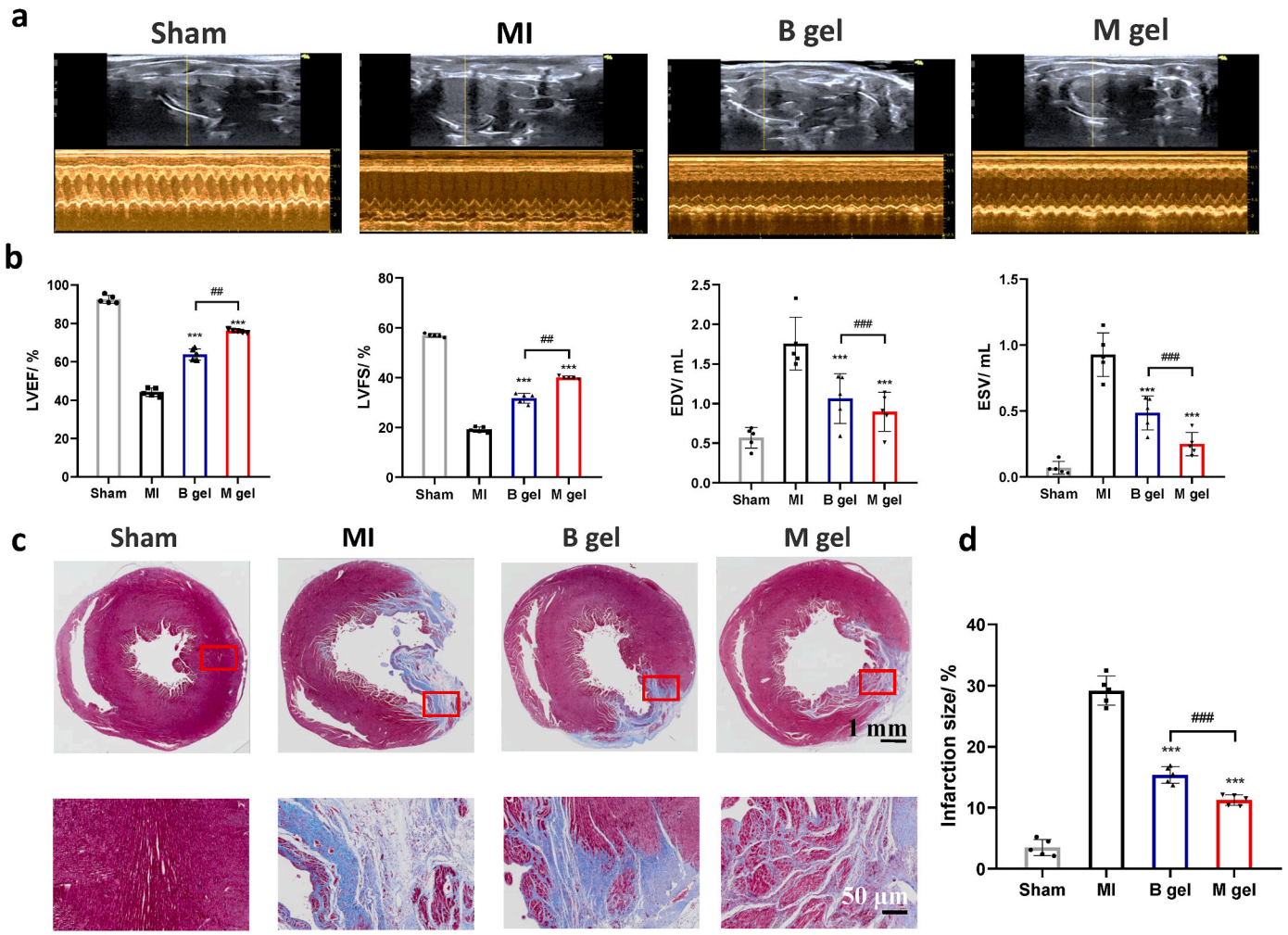

Fig. 6. M gel protects cardiac function and reduces myocardial fibrosis post MI in rats *in vivo*. (a) Representative echocardiography images. (b) Quantitative analysis of ventricular ejection fraction (LVEF), left ventricular fractional shortening (LVFS), left ventricular end-diastolic volume (EDV) and left ventricular end-systolic volume (ESV). (c) Representative Masson's trichrome staining images of the whole heart. Scale bars, 1 mm and 50 μm for the upper and lower images, respectively. (d) Quantitative analysis of infarcted size in the whole heart. $n = 5$ per group. ***$p < 0.001$ versus MI group; $^{\#\#}p < 0.01$ and $^{\#\#\#}p < 0.001$ between the selected groups.

systolic and diastolic inner left ventricular diameters (Fig. 6a and b). As expected, the M gel group showed the highest values for left ventricular ejection fraction (LVEF, 76.1 %) and left ventricular fractional shortening (LVFS, 40.1 %) compared with the B gel (63.8 % and 31.7 %) and MI (44.2 % and 19.2 %) groups, indicating the best improvement of left ventricular cardiac function. The end-systolic volume (ESV) and end-diastolic volume (EDV) values in the M gel group (0.90 mL and 0.25 mL) were the lowest compared with those of the B gel (1.06 mL and 0.48 mL) and MI (1.76 mL and 0.73 mL) groups, indicating the better cardiac function and less cardiac remodeling. Histological examination by Masson's trichrome staining (Fig. 6c) reveals the thicker left ventricle wall and more retained myocardium in the M gel-treated group. Compared to that in the MI and B gel groups, the fibrosis in the M gel group was effectively reduced (Fig. 6c and d), suggesting that the application of M gel immediately after MI can significantly alleviate the cardiomyocytes death and retain the healthy myocardium.

2.6. M gel promoted angiogenesis in a rat MI model

Revascularization is very important for post MI, which can reduce left ventricular remodeling and heart failure [53,54]. The antibodies against α-smooth muscle actin (α-SMA) and CD31 were employed to stain smooth muscle cells and endothelial cells, respectively, where the α-SMA$^+$/CD31$^+$ tubular structures represent new blood vessels. As shown in Fig. S9, a higher density of CD31$^+$/α-SMA$^+$ stained new vessels was observed in the M gel compared to other groups. Moreover, the relative expression of angiogenesis-related genes was also highest in the M gel-treated groups at 5 d post-surgery (Fig. S9c). In summary, the M gel treatment results in the significant vascularization compared to other treatment groups.

2.7. M gel protected cardiac function and reduced myocardial fibrosis in a minipig MI model

The clinically relevant therapy was testified in a minipig MI model due to the similarity of pigs to human being (Fig. 7a). The single photon emission computed tomography (SPECT) imaging was employed to study cardiac function after 28 d post MI (Fig. 7b). The LVEF and stroke volume (SV) of the M gel-treated groups were significantly increased (76.5 % and 29.8 mL) compared to those of the B gel (52.3 % and 26.8 mL) and MI (32.3 % and 14.3 mL) groups. Moreover, the ESV and EDV were much reduced from 70 mL to 39.3 mL–8.5 mL and 9 mL in the M gel group (Fig. 7c), which were also lower than those of the B gel group (47 mL and 24 mL).

Histologically, both Masson's trichrome and H&E staining (Fig. 7d and e) reveals that the distinct and thick muscle layers were remained in

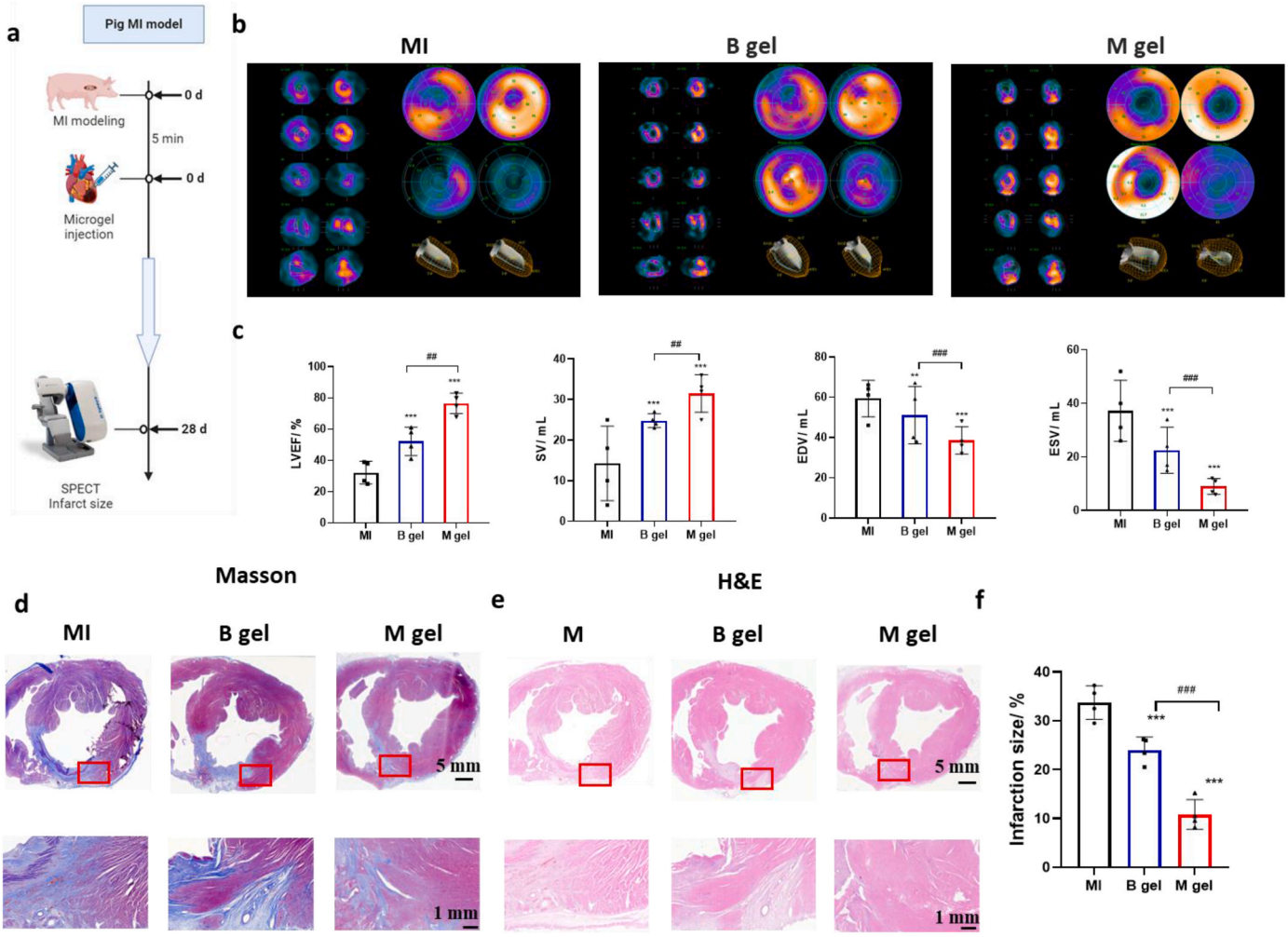

Fig. 7. M gel protects cardiac function and reduces myocardial fibrosis post MI in minipigs *in vivo*. (a) Timeline of the minipig MI study. (b) Representative SPECT images. (c) Quantitative analysis of LVEF, stroke volume (SV), EDV and ESV. Representative (d) Masson's trichrome and (e) H&E staining images of the whole heart. (f) Quantitative analysis of infarcted size in the whole heart. $n = 4$ per group. $^{**}p < 0.01$ and $^{***}p < 0.001$ versus MI group; $^{\#\#}p < 0.01$ and $^{\#\#\#}p < 0.001$ between the selected groups.

the infarcted areas of the M gel group. The moderately thickened muscle and the most obvious fibrillary layers were observed in the B gel and MI group, respectively. Reactive fibrosis is an interstitial deposition of collagens surrounding cardiomyocytes and myocardial fibers which can also be localized in the perivascular areas. A special subtype of cardiac fibrosis is termed "plexiform fibrosis", which is characterized by disorganized bundles of collagen fibers in areas of myocardial disarray. It is frequently observed at the insertion points of the right ventricle to the septum. Thus, the fibrotic area would not appear to be entirely in the left ventricle. Quantitative analysis showed approximately two times less fibrous content in the B gel group (~10.8 %) than in the MI group (~33.72 %) (Fig. 7f). These observations provide evidence that the M gel treatment most effectively attenuates the fibrosis and restricts the cardiac remodeling post MI.

By integrating the key functions of ROS-scavenging, microRNA delivery and microgel structure, the all in one system has the advantages of low viscosity for easy injection, assembly into porous scaffolds *in situ* to allow cell infiltration, ROS-scavenging that modulates the inflammatory microenvironment and reduces apoptosis, and finally based on these prerequisites the loaded microRNA can take the largest role to down-regulate PTEN and thus promote cardiomyocyte proliferation *in vivo*. Indeed, our oxidative stress-relief microgels loaded with miR-19a/b have exhibited a powerful effect on promoting cardiomyocyte proliferation and maintaining cardiac function to avoid long term heart failure. The selenoketal-based ROS-scavenging microgels very sensitively and effectively remitted oxidative stress in the infarct area, suppressed the acute inflammation and reduced the cardiomyocyte apoptosis in the early stages post MI, compared to the bulk counterpart. With the miR-19a/b continuously released from the microgels and ingested by cardiomyocytes, more cardiomyocytes turned into the cell cycle and proliferated. Consequently, the Ki67 and PH3-positive signals in the cardiomyocytes were significantly increased compared to previous work [48–52]. Taken together, our microgels exhibit prominent therapeutic effect on cardiac repair in both small-animal and minipig MI treatments, showing their great potential for clinical minimally invasive therapy.

The ultimate goal of complete cardiac repair is heart regeneration through cardiomyocytes renewal, fibrosis inhibition, muscle tissue retention and neovascularization. The cardiac regeneration is constituted by a series of complex and strictly controlled processes. The miRNAs-based treatment therapies have played an important role in the next-generation of *in situ* regenerative therapies for the heart. Especially, compared to other methods, miRNA mimics can be easily synthesized and delivered by viral and non-viral transfection methods. Nonetheless, current miRNA-based strategies for heart repair are vastly inefficient and only primarily tested in rodents. The better use of miRNAs in big animal even human being is extremely important yet challenging for MI treatment. Our study shows that selenoketal-based microgels loaded with miR-19a/b are not only easily delivered, but also significantly

maintain the function of miR-19a/b in boosting the cardiomyocyte proliferation to achieve strong therapeutic effects on both rats and minipigs, presenting a significant progress for treatment of MI in human being.

3. Materials and methods

3.1. Materials

The materials used are listed in Table 1. The water was purified by Millipore Milli-Q purification system for all experiments. CD-HDA was synthesized according to the method reported previously [55]. The photo-initiator (LAP) was also prepared according to the previous work [56].

3.2. Material preparation

Synthesis of selenoketal-NH_2: selenocysteamine dihydrochloride (6.38 g, 20 mM) and TECP (6.88 g, 24 mM) were dissolved in water (10 mL). After being stirred at room temperature (RT) for 30 min, 0.5 mL of HCl was added, followed by stirring at RT for another 30 min. The solution was then freeze-dried before it was dissolved in 15 mL of acetic acid. After 5 mL of acetone was added into the solution, it was stirred at RT for 12 h. During this process, large amount of white precipitates was formed. After extraction and filtration, the precipitates were added into 10 M NaOH solution to obtain a light-yellow emulsion. After separatory filtration, the light-yellow liquid product (selenoketal-NH_2) was obtained, which was stored at −80 °C.

Synthesis of HBPASe: the HBPASe was synthesized from PEGDA700 and selenoketal diamine [57,58]. In brief, PEGDA700 (3.08 g, 4.4 mmol), selenoketal diamine (0.58 g, 2 mmol), DMSO (10 mL) and TEA (10 μL) (2.2:1 M ratio of double bond to active hydrogen) were mixed and fully stirred in a single-neck flask for 30 min at RT, before it was placed in an oil-bath at 80 °C for 8 h under continuous stirring. After reaction, the product was obtained by precipitating with MTBE for 3 times. The precipitates was placed in a vacuum oven overnight to remove the residual MTBE and to obtain final HBPASe.

Synthesis of methacrylated HA (HAMA) [55]: HA (2.5 g) was fully dissolved in 125 mL water first. The pH of the HA solution was then adjusted to 8.5 by 1.0 M NaOH solution in an ice bath. MA (5.625 mL) was added into HA solution dropwise, while the pH was maintained by adding the NaOH solution. After reaction for 4 h, during which pH was maintained at 7.5–8.5, and then overnight at RT, the product was obtained by precipitating with ethyl alcohol for 3 times. After the solution was dialyzed against water for 7 d, it was frozen and lyophilized. The structure of HAMA was analyzed by ^{1}H nuclear magnetic resonance (NMR) spectroscopy (Bruker DMX-500, Switzerland).

Synthesis of HAMA-TBA: HAMA (3.0 g) was fully dissolved in 150 mL water. After 9.0 g Dowex 50W × 8 resin was added and stirred for 2 h, the solution was filtrated to remove residual resin, and the pH of solution was adjusted to 7.02–7.05 by TBA-OH solution [55]. The mixture was then frozen and lyophilized. The structure of HAMA-TBA was analyzed by ^{1}H NMR spectroscopy.

Synthesis of HAMA-CD: The HAMA-CD was prepared by amidation between cyclodextrin and HAMA-TBA with BOP [55]. Their structures were confirmed by ^{1}H NMR spectroscopy.

Table 1
Materials used in this work.

Materials	Suppliers
Poly (ethylene glycol) diacrylate (PEGDA700, Mn = 700)	Sigma-Aldrich, USA
Hyaluronic acid (HA, Mn = 100 kDa)	Dongyuan Biotechnology Co., Ltd, China
Sodium hydroxide (NaOH)	Sinopharm Chemical Reagent Co., Ltd, China
β-Cyclodextrin (CD)	
Sodium chloride (NaCl)	
Hydrochloric acid (40 % wt/vol in water, HCl)	
Triethylamine (TEA)	
Methyl tertiary butyl ether (MTBE)	
Hydrogen peroxide (10 %, H_2O_2)	
Acetone,	
Acetonitrile	
Diethyl ether	
Methanol	
Span™ 80	Aladin, China
n-Hexane	
Paraffin liquid	
Dowex 50W × 8 resin	
Tetrabutylammonium hydroxide solution (TBA-OH, 40 % wt/vol in water)	
Anhydrous dimethyl sulfoxide (DMSO)	
p-Toluenesulfonyl chloride (PTSC)	
(Benzotriazol-1-yloxy)tris(dimethylamino) phosphonium hexafluorophosphate (BOP)	
Tris(2-carboxyethyl)phosphine hydrochloride (TCEP)	
ammonium chloride (NH_4Cl)	
N,N-Dimethylformamide (DMF)	
1,1-Diphenyl-2-picrylhydrazyl (DPPH)	
1,6-Hexanediamine (HDA)	
Selenocystamine dihydrochloride	Bide Pharmaceutical Technology Co., Ltd, China
MiR-19a/b-cholesterol and miR-19a/b-Cy3	Ribobio Biotechnology Co., Ltd, China

3.3. Preparation of ROS-scavenging microgels and bulk hydrogel

The ROS-scavenging microgels loaded with miR-19a/b (M gel) were prepared by a customized microfluidic device from a hydrogel precursor, which was consisted of HBPASe (150 mg, 15 wt%), HAMA-CD (20 mg, 2 wt%), miR-19a/b (50/50 nmol) and LAP (0.5 wt%) per mL. Meanwhile, Span™ 80 and paraffin liquid were mixed by a volume ratio of 15:85, which acted as a surfactant and continuous oil phase. The hydrogel precursor flowed through a capillary tube with an inner diameter of 0.1 mm (Polymicro Technologies), with the flow rate at 400 μL h^{-1}. Meanwhile, the oil phase flowed out through a polyvinyl fluoride (ETFE) tube with an inner diameter of 0.5 mm, with the flow rate at 5 mL h^{-1}. The prepared microgels in ETFE tube were fully photo-crosslinked under UV irradiation for 5 min. Thereafter, the M gels were obtained through centrifugation, and washed with n-hexane, ethanol and water for 3 times, respectively.

The ROS-responsive bulk hydrogel loaded with miR-19a/b (B Gel) was prepared with the hydrogel precursor as aforementioned under UV irradiation for 30s.

3.4. Characterization of M gels

The M gels were imaged using an optical microscope (TS2-S-SM, Nikon) in water, and the freeze-dried M gels were imaged using a scanning electron microscope (SEM, S-4800, Hitachi). The size of the M gels was calculated using Image J software. The rheological property of hydrogels and microgels were characterized by a rotary rheometer (HAKE, MARS 60, US).

3.5. ROS-scavenging efficiency in vitro

For the scavenging of H_2O_2, 100 μL of M gel and B gel were incubated in 1 mL of 100 μM H_2O_2 solution for 30 min at 37 °C. Then, the 500 μL of solution was collected to react with 500 μL of 1 m KI solution in dark for another 5 min. The absorbance of final solution at 412 nm was measured by a microplate reader (Fluoroskan FL, Thermo Scientific). The absorbance curves of the final solutions were measured by a UV–vis spectroscopy (UV-2660i, Shimadezu, Japan).

For the DPPH radicals scavenging, 100 μL of M gel and B gel were incubated in 1 mL of 200 μM DPPH solution at 37 °C in dark. The absorbance of solutions at 517 nm and different time was measured by a

microplate reader. The absorbance curves of the solutions were measured by UV–vis spectroscopy.

For the superoxide anion ($\cdot O_2^-$) scavenging, we used a superoxide anion assay kit according to the manufacturer's instructions. The absorbance of solutions at 550 nm and different time was measured by a microplate reader.

3.6. Cytotoxicity in vitro

The Cell Counting Kit-8 assay was employed to evaluate the cytotoxicity of M gel and B gel. 200 μL of M gel and B gel were first incubated in 2 mL of high sugar Dulbecco's modified Eagle medium (DMEM) at 37 °C for 24 h. After sterilized through a 0.22 μm bacteria-retentive filter, DMEM was then mixed with 10 % fetal bovine serum (FBS) and 100 U penicillin/100 μg mL^{-1} streptomycin. Meanwhile, H9C2 were seeded at a density of 5×10^3 cells in a 96-well plate per well, and incubated at 37 °C for 24 h with the DMEM prepared above. After 4-h incubation with 100 μL of 10 % CCK-8 (Beyotime, China) containing DMEM in dark, the absorbance at 450 nm was measured using a microplate reader to calculate the cell viability.

3.7. The degradation behavior in vitro

After 1 mL of B gel and M gel were immersed in 5 mL of PBS for 12 h to reach the swelling equilibrium, they were incubated in 5 mL of PBS and 250 mM H_2O_2/PBS at 37 °C to detect the hydrolysis and ROS-responsive degradation properties, respectively. The wet weight of gels was measured along with time prolongation, and the solutions were replaced with fresh ones once a day, respectively.

3.8. Cell protection against oxidative stress in vitro

The H9C2 were seeded at a density of 1×10^5 cells in a 12-well plate per well. After 24 h, the medium was replaced with 500 μM H_2O_2 containing DMEM, and 500 μM H_2O_2 containing DMEM with B gel or M gel (200 μL), respectively. After 2 h, the H9C2 were stained by 2′,7′-dichlorodihydrofluorescein diacetate (DCFH-DA, Beyotime, China, 1:2000 v/v, in DMEM), a ROS fluorescent probe, for 30 min. After 3-time washes with PBS, H9C2 were collected, and measured by a flow cytometer (BD FACS Calibur, BD Biosciences, USA).

For cellular uptake of miR-19a/b detection, miR-19a/b (100 nM) containing DMEM was incubated with the cells for 3 h. After PBS washing, the fluorescence images were obtained by a fluorescence microscope (Fluoroskan FL, Thermo Scientific, USA). After 3-time washes with PBS, H9C2 were collected, whose fluorescence intensity was measured by a flow cytometer (BD FACS Calibur, BD Biosciences, USA).

3.9. MicroRNA release assay

1 mL of DMEM and DMEM containing 100 μM H_2O_2 were used to incubate 200 μL of M gel and B gel respectively. The supernatants were then collected and replaced with fresh DMEM at different time to test the miR-19a concentration by a RiboGreen RNA Assay Kit (ThermoFisher, USA). The fluorescence intensity was measured on a microplate reader (Ex 500 nm, Em 520 nm. Fluoroskan FL, Thermo Scientific, USA).

3.10. Rat MI model and hydrogel injection in vivo

The rat experiments were approved by the Experimental Animal Ethics Committee of Hangzhou Medical College following the Institutional Guidelines (ZJCLA-IACUC-20030156). The male SD rats (200 ± 20 g) were purchased from Zhejiang Academy of Medical Sciences. First, 1.7 mL of 4 % chloral hydrate was injected into each rat. After fully anesthetized, left lateral thoracotomy was performed, followed by ligation of the left anterior descending coronary artery (LAD) with a 6-0 silk suture. The infarct area of each rat was then injected with the M gel and B gel (80 μL). The volume of gels in the rat MI model was determined according to the dosage reported previously [59,60], where 80 μL of gels was appropriate. The volume of gels in minipig MI model was also determined according to a previous report [61]. The amount of miR-19a/b was determined according to the work reported in Ref. [48]. In a mice MI model, they used 110 μM mir-302b/c with 10 μL hydrogel. Thus we used miR-19a/b (50/50 nmol) per mL, that the concentration was about 100 μM miR-19Four groups were included: (1) Sham, (2) MI, (3) B gel, and (4) M gel. The M gel was easily injected without hindrance, whereas the B gel could also be injected into the myocardium under a significantly larger compression force.

The cardiac functions were examined by a VEVO2100 ultrasound system (Visual Sonics, Canada) at day 28 after surgery, and then were measured from 2D long-axis under M-mode.

3.11. Porcine MI model and hydrogel injection in vivo

The porcine experiment was approved by the Experimental Animal Ethics Committee of Peking University (LA2022377). First, tiletamine hydrochloride (4 mg/kg) and zolazepam hydrochloride (4 mg/kg) were employed to anesthetize the Bama minipigs (30–35 kg). The pericardium was then opened by a left thoracotomy. To establish the MI model, the second angular branch of left anterior descending branch (LAD) was ligated. The M gel and B gel were injected into the infarct region (9 injection sites, 100 μL per site), respectively.

The cardiac functions were examined by the VERITON-CT 400 system (Israel). Then, the function parameters, including LVEF, SV, EDV and ESV were calculated.

3.12. Histological analyses

The rat hearts and minipig hearts were harvested at day 28 after treatment, followed with PBS and 10 % KCl washing before they were fixed in 4 % formaldehyde for 48 h. The hearts were finally cut into paraffin sections. The collagen deposition and fibrosis level of infarcted hearts were studied by Masson's trichrome and H&E staining. The images were captured on a whole slide image scanner (Olympus Digital Slice Scanner VS200, Olympus, VS200, Japan). Image J software and GraphPad Prism software were used to analyze the data.

To evaluate the cardiomyocyte proliferation, Ki67 (abcam, ab15580), PH3 (cell Signaling, 9701) and Aurora B kinase (abcam, ab2254)-labeling assays were used to stain the rat hearts harvested at 5 d post-surgery. To observe the inflammation at 5 day, CD163 (abcam, ab182422) and CD86 (abcam, ab220188) immunofluorescent staining was performed. To study the vascularization after 28 days, the α-SMA (abcam, ab7817) and CD31 (abcam, ab24590) immunofluorescent staining was also carried out. The images were also captured on a whole slide image scanner. Image J software and GraphPad Prism software were used to analyze the data.

3.13. Quantitative Real-time PCR

The total RNAs were isolated from the rat heart after 5 day treatment by using TRIzol Reagent (Invitrogen). The 1.0 μg of RNA was reverse-transcribed into cDNA by using the Prime Script RT reagent kit with gDNA Eraser (TaKaRa) in the PCR instrument (Veriti 96-Well Thermal Cycler, Veriti). The obtained cDNA was then used in quantitative PCR to quantify the transcription of target proteins using the SYBR Premix Ex TaqII kit (TaKaRa) in a CFX 96 Bio-Rad (CFX96 Touch, Bio-Rad, USA). The studied genes and their sequences of rat-related gene primers are listed in Table S1.

3.14. Statistical analyses

All statistical analyses were performed in Graphpad Prism 7. All data are reported as mean ± standard deviation (SD), and the repeating

numbers are reported in figure captions. The significant difference was tested with One-way ANOVA and post-hoc least significant difference (LSD) test. The difference was considered statistically significant when $p < 0.05$.

CRediT authorship contribution statement

Kai Wang: Writing – review & editing, Writing – original draft, Visualization, Validation, Methodology, Investigation, Formal analysis, Data curation. **Jun Wen:** Writing – review & editing, Writing – original draft, Visualization, Validation, Methodology, Investigation, Formal analysis, Data curation, Conceptualization. **Wen-Yao Wang:** Writing – review & editing, Writing – original draft, Visualization, Validation, Methodology, Investigation, Formal analysis, Data curation, Conceptualization. **Kefei Zhao:** Writing – review & editing, Writing – original draft, Visualization, Validation, Methodology, Investigation, Formal analysis, Data curation, Conceptualization. **Tong Zhou:** Methodology, Investigation. **Shunqin Wang:** Methodology, Investigation. **Qiaoxuan Wang:** Methodology, Investigation. **Liyin Shen:** Methodology, Investigation. **Yanxin Xiang:** Methodology, Investigation. **Tanchen Ren:** Methodology, Investigation. **Jinghai Chen:** Writing – review & editing, Supervision, Resources, Funding acquisition. **Yi-Da Tang:** Writing – review & editing, Supervision, Resources, Funding acquisition, Conceptualization. **Yang Zhu:** Writing – review & editing, Supervision, Resources, Funding acquisition, Conceptualization. **Changyou Gao:** Writing – review & editing, Supervision, Resources, Project administration, Funding acquisition, Conceptualization.

Data availability

The raw/processed data required to reproduce these findings cannot be shared at this time due to technical or time limitations.

Ethics approval and consent to participate

The rat experiments were approved by the Experimental Animal Ethics Committee of Hangzhou Medical College following the Institutional Guidelines (ZJCLA-IACUC-20030156).

The porcine experiment was approved by the Experimental Animal Ethics Committee of Peking University (LA2022377).

Declaration of interests

The authors declare that they have no known competing financial interests or personal relationships that could have appeared to influence the work reported in this paper.

Acknowledgements

We thank Jean-Marie Lehn for his valuable discussion and suggestions. This study is financially supported by the Joint Fund of National Natural Science Foundation of China (U22A20155), the Lingyan Program of Zhejiang Province (2022C01106), the State Key Laboratory of Transvascular Implantation Devices (012024004), the Postdoctoral Researcher Program in China (GZC20232244, 2023M742975), and the 111 Project (B16042).

Appendix A. Supplementary data

Supplementary data to this article can be found online at https://doi.org/10.1016/j.bioactmat.2025.02.004.

References

[1] S. Frantz, M.J. Hundertmark, J. Schulz-Menger, F.M. Bengel, J. Bauersachs, Eur. Heart J. 43 (2022) 2549.
[2] G.K. Kolluru, R.E. Shackelford, X. Shen, P. Dominic, C.G. Kevil, Nat. Rev. Cardiol. 20 (2023) 109–125.
[3] Y. Saito, K. Oyama, K. Tsujita, S. Yasuda, Y. Kobayashi, J. Cardiol. 81 (2023) 168–178.
[4] A. Camaj, V. Fuster, G. Giustino, S.W. Bienstock, D. Sternheim, R. Mehran, G. D. Dangas, A. Kini, S.K. Sharma, J. Halperin, M.R. Dweck, M.E. Goldman, J. Am. Coll. Cardiol. 79 (2022) 1010–1022.
[5] J. He, D. Liu, L. Zhao, D. Zhou, J. Rong, L. Zhang, Z. Xia, Exp. Ther. Med. 23 (2022) 11357.
[6] A.M. Garvin, L.C. Katwa, Am. J. Physiol. Heart Circ. Physiol. 325 (2023) 869–881.
[7] S.N. Ricketts, L. Qian, J. Mol. Cell. Cardiol. 172 (2022) 90–99.
[8] B. Laggerbauer, S. Engelhardt, J. Clin. Investig. 132 (2022) 3009008.
[9] G. Passacquale, P. Sharma, D. Perera, A. Ferro, Br. J. Clin. Pharmacol. 88 (2022) 2686–2699.
[10] E. van Rooij, E.N. Olson, Nat. Rev. Drug Discov. 11 (2012) 860–872.
[11] G.B. Lim, Nat. Rev. Cardiol. 16 (2019) 454.
[12] B. Liu, B. Wang, X. Zhang, R. Lock, T. Nash, G. Vunjak-Novakovic, Sci. Transl. Med. (2021) 13.
[13] V. Shah, J. Shah, Frontiers in Cardiovascular Medicine, vol. 9, 2022 835138.
[14] K. Gabisonia, G. Prosdocimo, G.D. Aquaro, L. Carlucci, L. Zentilin, I. Secco, H. Ali, L. Braga, N. Gorgodze, F. Bernini, S. Burchielli, C. Collesi, L. Zandona, G. Sinagra, M. Piacenti, S. Zacchigna, R. Bussani, F.A. Recchia, M. Giacca, Nature 569 (2019) 418.
[15] F. Gao, M. Kataoka, N. Liu, T. Liang, Z.-P. Huang, F. Gu, J. Ding, J. Liu, F. Zhang, Q. Ma, Y. Wang, M. Zhang, X. Hu, J. Kyselovic, X. Hu, W.T. Pu, J.a. Wang, J. Chen, D.-Z. Wang, Nat. Commun. 10 (2019) 1802.
[16] J. Chen, Z.-P. Huang, H.Y. Seok, J. Ding, M. Kataoka, Z. Zhang, X. Hu, G. Wang, Z. Lin, S. Wang, W.T. Pu, R. Liao, D.-Z. Wang, Circ. Res. 112 (2013) 1557.
[17] Y. Fu, J. Chen, Z. Huang, ExRNA 1 (2019) 1–14.
[18] S. Huang, Y. Zhou, Y. Zhang, N. Liu, J. Liu, L. Liu, C. Fan, Cardiovasc. Drugs Ther. 39 (2025) 221–232.
[19] N. Carballo-Pedrares, I. Fuentes-Boquete, S. Díaz-Prado, A. Rey-Rico, Pharmaceutics 12 (2020) 752.
[20] K. Wang, J. Wen, T. Liang, H. Hu, S. Li, L. Shen, T. Ren, Y. Yao, J. Xie, J. Ding, J. Chen, Y.-D. Tang, Y. Zhu, C. Gao, Biomaterials 312 (2025) 122732.
[21] L.L. Wang, Y. Liu, J.J. Chung, T. Wang, A.C. Gaffey, M. Lu, C.A. Cavanaugh, S. Zhou, R. Kanade, P. Atluri, Nat. Biomed. Eng. 1 (2017) 983–992.
[22] Z. Zheng, Y. Tan, Y. Li, Y. Liu, G. Yi, C.-Y. Yu, H. Wei, J. Contr. Release 335 (2021) 216–236.
[23] X. Zhang, W. Liu, Adv. NanoBiomed Res. 2 (2022) 2200008.
[24] T. Wu, W. Liu, NPG Asia Mater. 14 (2022) 103968, 9.
[25] L. Huang, J. Wang, L. Kong, X. Wang, Q. Li, L. Zhang, J. Shi, J. Duan, H. Mu, Int. J. Biol. Macromol. 222 (2022) 1476–1486.
[26] Z. Zheng, C. Lei, H. Liu, M. Jiang, Z. Zhou, Y. Zhao, C.Y. Yu, H. Wei, Adv. Healthcare Mater. 11 (2022) e2200990.
[27] H.-t. Shi, Z.-h. Huang, T.-z. Xu, A.-j. Sun, J.-b. Ge, EBioMedicine 78 (2022) 103968.
[28] Q. Feng, D. Li, Q. Li, X. Cao, H. Dong, Bioact. Mater. 9 (2022) 105–119.
[29] K. Wang, Z. Wang, H. Hu, C. Gao, Supramole. Mater. 1 (2022) 100006.
[30] Y. Kittel, A.J. Kuehne, L. De Laporte, Adv. Healthcare Mater. 11 (2022) 2101989.
[31] R. Breslow, B.L. Zhang, J. Am. Chem. Soc. 118 (1996) 8495–8496.
[32] C. Wolfrum, S. Shi, K.N. Jayaprakash, M. Jayaraman, G. Wang, R.K. Pandey, K. G. Rajeev, T. Nakayama, K. Charrise, E.M. Ndungo, T. Zimmermann, V. Koteliansky, M. Manoharan, M. Stoffel, Nat. Biotechnol. 25 (2007) 1149–1157.
[33] Y.M. Liu, Y. Xia, W. Dai, H.Y. Han, Y.X. Dong, J. Cai, X. Zeng, F.Y. Luo, T. Yang, Y. Z. Li, J. Chen, J. Guan, BMC Cancer 14 (2014) 889.
[34] J. Sun, J. Li, Z. Huan, S.J. Pandol, D. Liu, L. Shang, L. Li, Adv. Funct. Mater. 33 (2023) 202211897.
[35] M. Bhattacharjee, J.L.E. Ivirico, H.-M. Kan, S. Shah, T. Otsuka, R. Bordett, M. Barajaa, N. Nagiah, R. Pandey, L.S. Nair, C.T. Laurencin, Proc. Natl. Acad. Sci. U. S. A 119 (2022) e2120968119.
[36] H. Zhou, C. Liang, Z. Wei, Y. Bai, S.B. Bhaduri, T.J. Webster, L. Bian, L. Yang, Mater. Today 28 (2019) 81–97.
[37] D. Jin, Q. Wang, K.F. Chan, N. Xia, H. Yang, Q. Wang, S.C.H. Yu, L. Zhang, Sci. Adv. 9 (2023) eadf9278.
[38] C. Doescher, A. Thai, E. Cha, P.V. Cheng, D.K. Agrawal, F.G. Thankam, Gels 8 (2022) 576.
[39] M.N. Sayegh, K.A. Cooney, W.M. Han, M. Cicka, F. Strobel, L. Wang, A.J. Garcia, R. D. Levit, J. Mol. Cell. Cardiol. 176 (2023) 98–109.
[40] X. Hong, A.C. Luo, I. Doulamis, N. Oh, G.-B. Im, C.-Y. Lin, P.J. Del Nido, R.-Z. Lin, J.M. Melero-Martin, Adv. Healthcare Mater. (2023) e2301581.
[41] Y. Yao, H. Zhang, Z. Wang, J. Ding, S. Wang, B. Huang, S. Ke, C. Gao, J. Mater. Chem. B 7 (2019) 5019–5037.
[42] G. Saravanakumar, J. Kim, W.J. Kim, Adv. Sci. 4 (2017) 1600124.
[43] C. Mian, Y. Zhen, Q. Lifen, Y. Yi, D. Yulei, Z. Cuntai, M. Tao, Gene 851 (2023) 147030.
[44] W. Mi, S. Tang, S. Guo, H. Li, N. Shao, Chin. Chem. Lett. 33 (2022) 1331–1336.
[45] M. Nie, J. Liu, Q. Yang, H.Y. Seok, X. Hu, Z.L. Deng, D.Z. Wang, Cell Death Dis. 7 (2016) e2261.
[46] K.J. Mavrakis, A.L. Wolfe, E. Oricchio, T. Palomero, K. de Keersmaecker, K. McJunkin, J. Zuber, T. James, K. Chang, A.A. Khan, C.S. Leslie, J.S. Parker, P. J. Paddison, W. Tam, A. Ferrando, H.-G. Wendel, Nat. Cell Biol. 12 (2010) 372.
[47] Y.-h. Gao, J.-y. Qian, Z.-w. Chen, M.-q. Fu, J.-f. Xu, Y. Xia, X.-f. Ding, X.-d. Yang, Y.-y. Cao, Y.-z. Zou, J. Ren, A.-j. Sun, J.-b. Ge, Toxicol. Lett. 257 (2016) 72–83.
[48] L.L. Wang, Y. Liu, J.J. Chung, T. Wang, A.C. Gaffey, M. Lu, C.A. Cavanaugh, S. Zhou, R. Kanade, P. Atluri, E.E. Morrisey, J.A. Burdick, Nat. Biomed. Eng. 1 (2017) 983.

[49] T.M.A. Mohamed, Y.-S. Ang, E. Radzinsky, P. Zhou, Y. Huang, A. Elfenbein, A. Foley, S. Magnitsky, D. Srivastava, Cell 173 (2018) 104.
[50] D. Zhang, J. Ning, T. Ramprasath, C. Yu, X. Zheng, P. Song, Z. Xie, M.-H. Zou, Nat. Commun. 13 (2022) 6371.
[51] J. Sun, L. Wang, R.C. Matthews, G.P. Walcott, Y.-A. Lu, Y. Wei, Y. Zhou, L. Zangi, J. Zhang, Circ. Res. 133 (2023) 484–504.
[52] W. Chen, D. Pretorius, Y. Zhou, J. Zhang, Circulation 144 (2021) 9369.
[53] X. Zhang, Y. Lyu, Y. Liu, R. Yang, B. Liu, J. Li, Z. Xu, Q. Zhang, J. Yang, W. Liu, Nano Today 39 (2021) 101227.
[54] H.K. Awada, D.W. Long, Z. Wang, M.P. Hwang, K. Kim, Y. Wang, Biomaterials 125 (2017) 65–80.
[55] J.E. Mealy, J.J. Chung, H.-H. Jeong, D. Issadore, D. Lee, P. Atluri, J.A. Burdick, Adv. Mater. 30 (2018) 1705912.
[56] L.S.S.M. Magalilaes, F.E. Paz Santos, C.d.M. Vaz Elias, S. Afewerki, G.F. Sousa, A.S. A. Furtado, F.R. Marciano, A.O. Lobo, J. Funct. Biomater. 11 (2020) 12.
[57] J. Ding, Y. Yao, J. Li, Y. Duan, J.R. Nakkala, X. Feng, W. Cao, Y. Wang, L. Hong, L. Shen, Z. Mao, Y. Zhu, C. Gao, Small (2020) 16.
[58] S. Liang, Y. Zhang, H. Wang, Z. Xu, J. Chen, R. Bao, B. Tan, Y. Cui, G. Fan, W. Wang, W. Wang, W. Liu, Adv. Mater. 30 (2018) 2005038.
[59] J. Ding, Y. Yao, J. Li, Y. Duan, J.R. Nakkala, X. Feng, W. Cao, Y. Wang, L. Hong, L. Shen, Small 16 (2020) 2005038.
[60] K. Wang, J. Wen, T. Liang, H. Hu, S. Li, L. Shen, T. Ren, Y. Yao, J. Xie, J. Ding, Biomaterials 312 (2025) 122732.
[61] Y. Li, X. Chen, R. Jin, L. Chen, M. Dang, H. Cao, Y. Dong, B. Cai, G. Bai, J. J. Gooding, Sci. Adv. 7 (2021) eabd6740.